

Fig. 1. Possible poor fit-up experimental setups found in the literature (Jou, 2003; Cho et al., 2006).

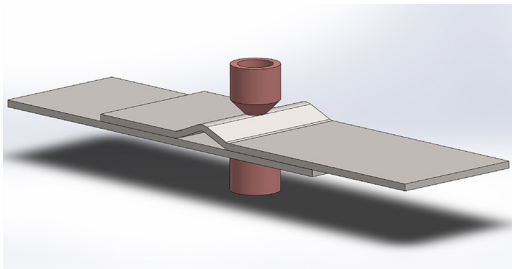


Fig. 2. Poor fit-up experimental setup.

## 2. Theoretical background

Although other poor fit-up simulation experimental setups have been used (see Fig. 1), in our case a decision was made to use weld specimens deformed into a triangular shape. The setups shown in Fig. 1 are namely based on the insertion of a foreign object between the weldpieces. This object stays there during the welding process and therefore does not reflect the reality very well. In our opinion during welding process there should be no object between the weldpieces. Therefore an experiment, a 3D model of which is shown in Fig. 2, is preferred. Whereas lower weldpiece is of normal (non-deformed) shape, the upper one is deformed in such a way that there is a triangular shaped bulge present in the place where the upper weldpiece will be pressed on by the upper electrode. In order to make this kind of deformity a special purpose tool was made (see Fig. 3). It has three pins which are welded to a metal sheet in such a way that a weldpiece can be inserted between the pins. The pins have to be long enough in order that they deform elastically when the tool together with the weldpiece is inserted into a vise and the vise jaws are pressed. The resulting weldpiece is shown in Fig. 4. Tools with different distances between pins (parameter  $d$  in Fig. 4) were made. The appropriate range of parameter  $d$  was



Fig. 3. The tool inserted into the vise.

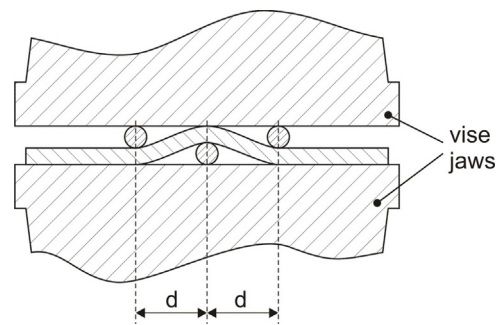


Fig. 4. Sample preparation using a vise.

determined based on the simulations performed in Ansys. The Ansys model was made in order to study the contact between the weldpieces after the weld force is applied. Due to symmetry a 3D half model was used (see Fig. 5). For weldpieces a bilinear elasto-plastic material model was used with tangential module of 2000 MPa, and the yield point of 235 MPa. The surface-to-surface contact elements (TARGE170 and CONTA174) were used for modeling of mechanical contacts and sliding between two steel sheets, and between sheets and electrodes. A high quality mapped mesh was ensured comprising of brick shaped finite elements only (Fig. 5). The element size between 0.5 mm and 1.0 mm is small in comparison with the thickness of the steel plates assuring 4 elements along the thickness. The result (Mises equivalent stress) is shown in Fig. 6. The most important conclusion of this analysis is the fact that despite the plastic deformation (gray color) there is a gap between the weldpieces. The same experiment was made for different values of parameter  $d$  and in accordance with the expectations the size of the gap depends on this parameter.

In order not only to detect but also to quantify the intensity of the poor fit-up condition, the welding force during the initial contact between the electrode tips and the weldpieces was measured. An assumption was made that the intensity of the deformation (parameter  $d$ ) must be related to the welding force curve, because the deformity acts like a spring with a certain spring constant.

As it is well known that poor fit-up in general implies smaller welding nugget and consequently inferior weld strength, the influence of a significant preheating on the weld strength has also been researched. For that purpose we applied the welding current profile shown in Fig. 7. It was assumed that the intensity of the welding current during preheating stage might influence the resulting weld strength. The logic behind this assumption is the fact that Young

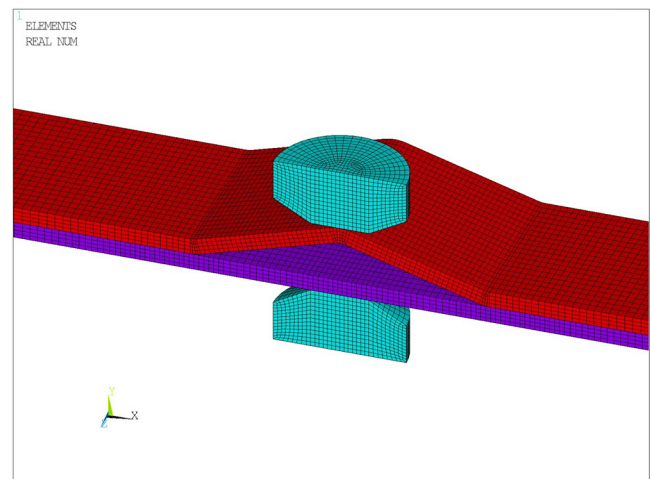


Fig. 5. The meshed finite element model.

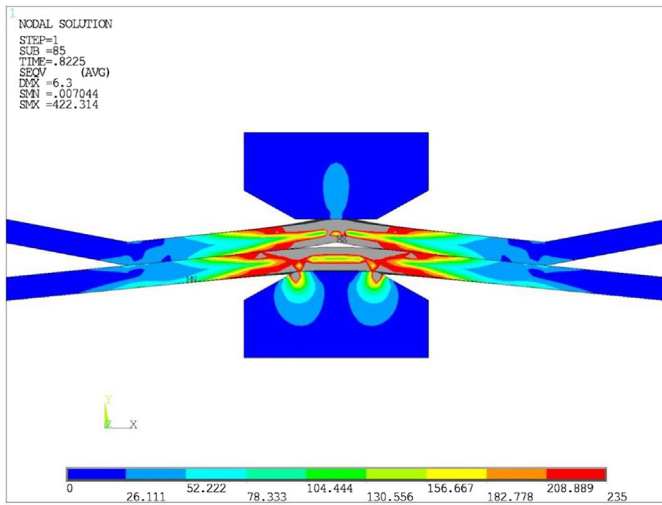


Fig. 6. The result of the simulation in Ansys.

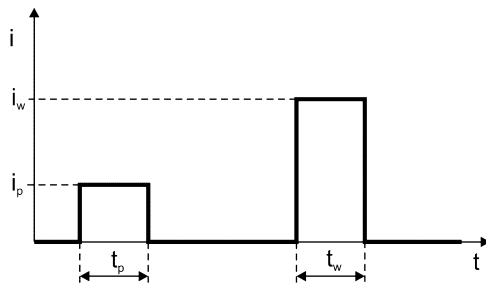


Fig. 7. Current during welding process (preheating and welding stage).

modulus decreases with temperature. Lower Young modulus however makes it possible to press the weldpieces together in such a way that the gap disappears or at least becomes smaller.

### 3. Experimental setup

The experiments were performed using a Gorenje Varstroj TIP VST 40 welding machine in combination with a Matuschek AutoSPATZM600L Medium Frequency Inverter Power Source. The weldpieces were 2 mm thick specimens cut out of mild steel sheets (St37). Electrode tips were type C caps according to DIN 44759 ( $d_1 = 7 \text{ mm}$ ,  $d_2 = 16 \text{ mm}$ ,  $l_1 = 16 \text{ mm}$ ,  $l_2 = 20 \text{ mm}$ ). The welding time and the preheating time were both equal to  $t_p = t_w = 300 \text{ ms}$ , the squeeze time was 1.5 s and the hold time 0.5 s. The time between preheating and welding was 2 s. The welding force was equal to  $F_w = 3 \text{ kN}$ . It was measured using a piezoelectric sensor (KIAG SWISS Type 903A) and a charge amplifier (Kistler Type 5006). The

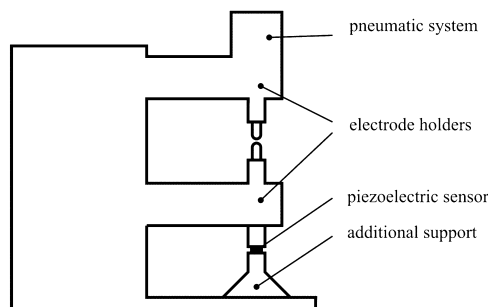


Fig. 8. Schematic representation of welding force measurement.

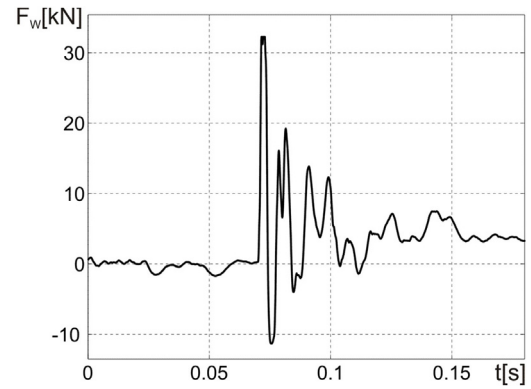


Fig. 9. Welding force during the initial contact between electrode tip and steel sheet for a non-deformed (good fit-up) sheet.

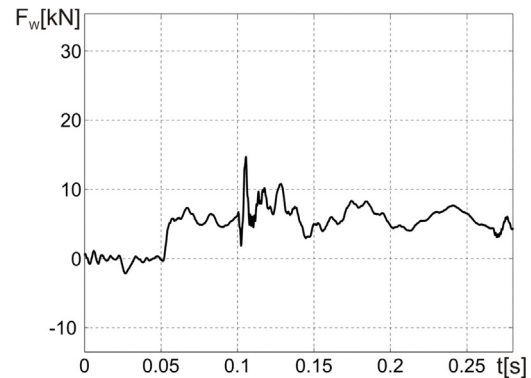


Fig. 10. Welding force during the initial contact between electrode tip and steel sheet for a deformed (poor fit-up) sheet.

mounting of the sensor is shown schematically in Fig. 8. The weld strength was measured using 120 mm × 40 mm specimens. They were tested on a ZWICK ROELL Z050 machine using tensile-shear testing (ISO 14273:2000). In order to get some estimate of the weld strength distribution three different welds were made at each preheating current setting.

### 4. Results

A typical welding force curve during the initial contact between the electrode tips and weldpieces for a normal (good fit-up) weld is shown in Fig. 9. Fig. 10 on the other hand shows a welding force curve for a case of very poor fit-up (small value of

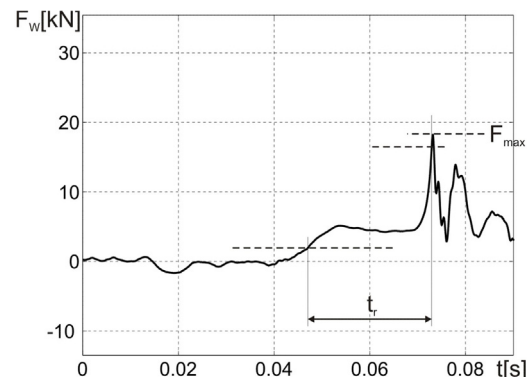


Fig. 11. The parameters used to estimate the extent of sheet deformation.



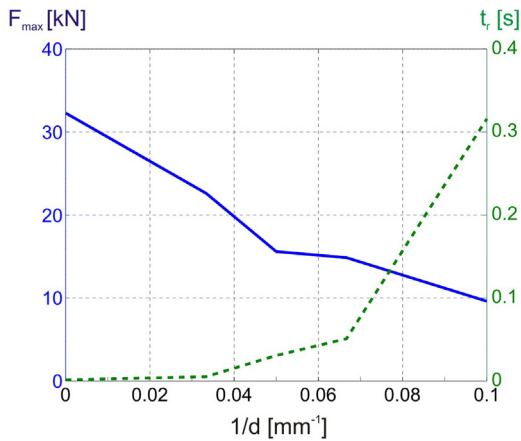


Fig. 12. Maximum welding force and rising time vs deformation.

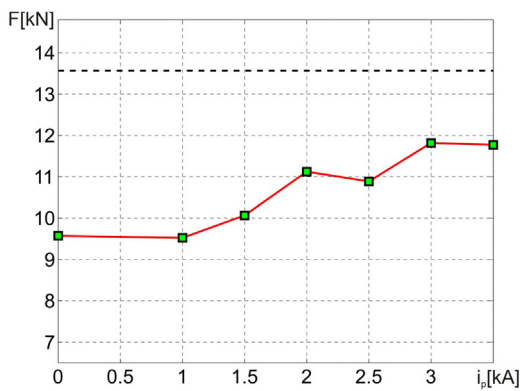


Fig. 13. Weld strength vs preheating current for a low intensity deformation (parameter  $d=30$  mm).

parameter  $d$  in Fig. 4). Based on these two figures it can be concluded that poor fit-up acts as a kind of cushion when the electrode tips come into contact with the weldpieces. In order to quantify the effect of this “cushioning”, two parameters were analyzed (see Fig. 11). The first parameter was the maximum of the welding force  $F_{max}$  and the second one was the rising time  $t_r$ . In accordance with the common definition of the rising time in control theory, it was defined as the time needed for the welding force to get from 10% of the maximum value to 90% of the maximum value. Five different values of parameter  $d$  were analyzed; 10 mm, 15 mm, 20 mm, 30 mm, and non-deformed case, where we can assume  $d=\infty$ . For

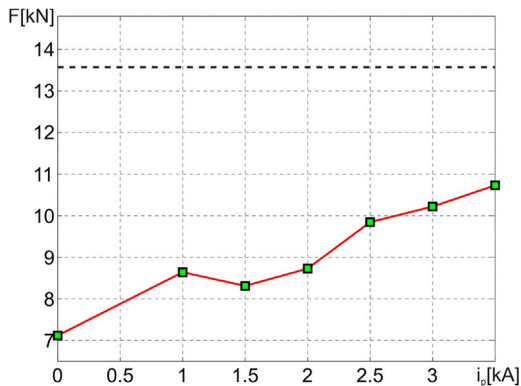


Fig. 14. Weld strength vs preheating current for a high intensity deformation (parameter  $d=10$  mm).

each value of parameter  $d$ , 10 experiments were made and average values for maximum welding force  $F_{max}$  and the rising time  $t_r$  were calculated. The results are shown in Fig. 12. The parameter  $d^{-1}$  is put on the  $x$ -axis, because it is impossible to plot an infinite value. Another reason is the fact that if  $d^{-1}$  is plotted on  $x$ -axis instead of  $d$ , the intensity of deformation is increasing from left to right and  $d^{-1}=0$  is the non-deformed case. It can be seen that especially maximum welding force can be used as a good estimate of the intensity of poor fit-up condition. The sensitivity of the parameter remains fairly constant throughout the range of the parameter  $d^{-1}$  taken in consideration. Rising time on the other hand exhibits very good sensitivity for very deformed welds (small value of  $d$  which means large value of  $d^{-1}$ ). Its low sensitivity in the case of slightly deformed welds however limits its applicability.

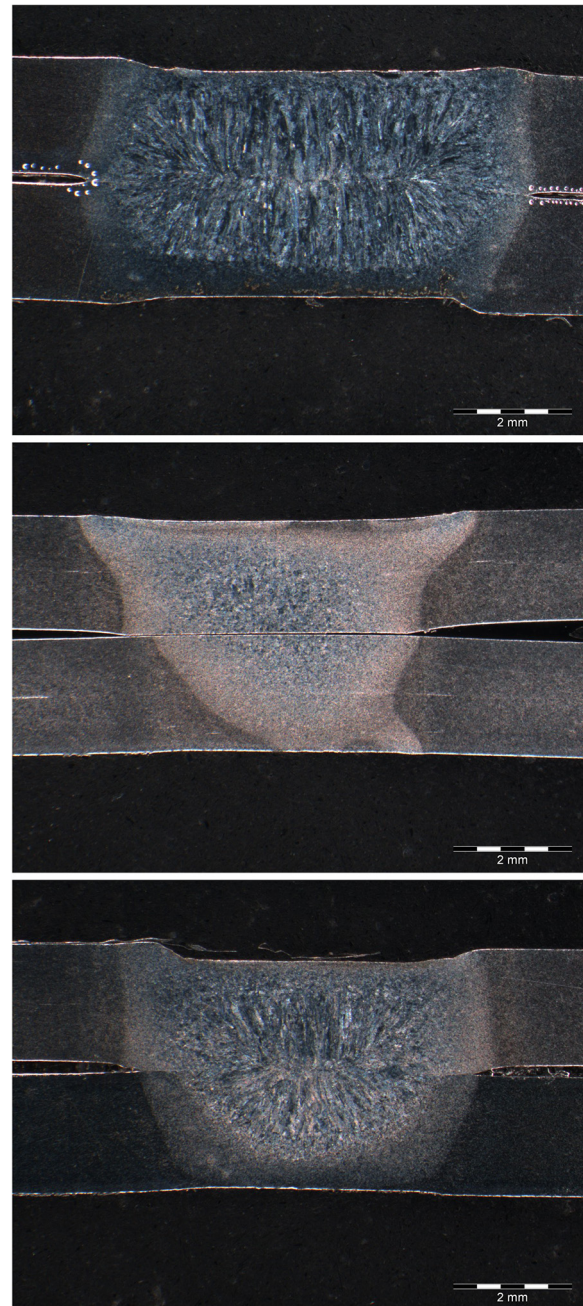


Fig. 15. Micrographs for three cases: non-deformed (top), deformed (middle), deformed with preheating current  $i_p=3$  kA (bottom).

In order to test the possibility of limiting the decrease in weld strength due to poor fit-up condition, the influence of preheating current  $i_p$  (see Fig. 7) on weld strength  $F$  was analyzed. The welding current  $i_w$  was 7 kA and both the preheating and welding time were equal to 300 ms. The results obtained for the case of low intensity deformation (parameter  $d = 30$  mm) are shown in Fig. 13. It can be seen that in general increased preheating current increases the resulting weld strength. The preheating current was increased in 0.5 kA steps until it reached 3.5 kA, because at 4 kA the weldpieces were already welded. The same experiment was also made for the case of high intensity deformation (parameter  $d = 10$  mm). The results are shown in Fig. 14. The same general trend of increased weld strength with increasing preheating current can be observed here as well. The only major difference is that the whole weld strength curve is lower than in the case of the less deformed weldpiece. In both figures a dashed line denoting the weld strength of a non-deformed weldpiece case is added. It can be seen that although the preheating makes it possible to increase the weld strength in both cases, it is still significantly below the non-deformed case.

In order to analyze this behavior the micrographs for three different cases are presented (see Fig. 15). The top photo shows the non-deformed case. The photo in the middle shows the high intensity of deformation case without preheating. It can be seen that in this case the nugget is not even fully developed. Such a case definitely exhibits inferior weld strength. The bottom photo shows the case of the spot weld with high intensity of deformation and the preheating current of  $i_p = 3$  kA. The nugget is clearly seen, but its size is smaller than in the non-deformed case (top photo). Therefore the resulting weld strength is lower. It should however be emphasized that the resulting inferior weld strength in the case of the deformed spot welds cannot be attributed only to the weld nugget size. As clearly seen in Fig. 6, the lower weldpiece deforms as well during the initial contact. This implies a significant amount of tensile stress during tensile-shear testing which of course results in a lower weld strength.

## 5. Conclusions

Based on the presented research the following conclusions can be made:

- The proposed experimental setup makes it possible to simulate poor fit-ups of different intensities.
- By measuring the welding force during the initial contact between the electrode tips and the weldpieces it is possible to estimate the intensity of the poor fit-up condition.

- Additional preheating phase can improve the weld strength of the deformed welds. It is however still far below the levels of weld strength achieved by non-deformed welds. It can therefore be concluded that in practice if the poor fit-up condition is observed (especially in the case of significant deformation) it is better to make a spot weld in a place nearby, where the weldpiece is not deformed.

In our research the deformity considered was of triangular shape. For future research it would be interesting to design an experiment which would be able to simulate random geometrical nature of the deformity, which would resemble the real environment even more.

## References

- Cho, Y., Li, W., Hu, S., 2006. Design of experiment analysis and weld lobe estimation for aluminum resistance spot welding. *Weld. J.* 85, 45–S–51–S.
- Ikeda, R., Okita, Y., Ono, M., Yasuda, K., Terasaki, T., 2014. Development of advanced resistance spot welding process using control of electrode force and welding current during welding. *Weld. Int.* 28, 13–20.
- Jou, M., 2003. Real time monitoring weld quality of resistance spot welding for the fabrication of sheet metal assemblies. *J. Mater. Process. Technol.* 132, 102–113.
- Luo, Y., Li, J., Wu, W., 2013. Nugget quality prediction of resistance spot welding on aluminum alloy based on structureborne acoustic emission signals. *Sci. Technol. Weld. Join.* 18, 301–306.
- Martín, Ó., Pereda, M., Santos, J.I., Galán, J.M., 2014. Assessment of resistance spot welding quality based on ultrasonic testing and tree-based techniques. *J. Mater. Process. Technol.* 214, 2478–2487.
- Podržaj, P., Simončič, S., 2013. Resistance spot welding control based on the temperature measurement. *Sci. Technol. Weld. Join.* 18, 551–557.
- Podržaj, P., Polajnar, I., Diaci, J., Kariž, Z., 2004. Expulsion detection system for resistance spot welding based on a neural network. *Meas. Sci. Technol.* 15, 592–598.
- Podržaj, P., Polajnar, I., Diaci, J., Kariž, Z., 2005. Estimating the strength of resistance spot welds based on sonic emission. *Sci. Technol. Weld. Join.* 10, 399–405.
- Podržaj, P., Polajnar, I., Diaci, J., Kariž, Z., 2008. Overview of resistance spot welding control. *Sci. Technol. Weld. Join.* 13, 215–224.
- Podržaj, P., Simončič, S., 2011. Resistance spot welding control based on fuzzy logic. *Int. J. Adv. Manuf. Technol.* 52, 959–967.
- Simončič, S., Podržaj, P., 2014. Resistance spot weld strength estimation based on electrode tip displacement/velocity curve obtained by image processing. *Sci. Technol. Weld. Join.* 19, 468–475.
- Zhang, H., Wang, F., Gao, W., Hou, Y., 2014. Quality assessment for resistance spot welding based on binary image of electrode displacement signal and probabilistic neural network. *Sci. Technol. Weld. Join.* 19, 242–249.
- Zhang, Y., Shen, J., Lai, X., 2012. Influence of electrode force on weld expulsion in resistance spot welding of dual phase steel with initial gap using simulation and experimental method. *ISIJ Int.* 52, 493–498.
- Zhao, D., Wang, Y., Lin, Z., Sheng, S., 2013. Quality monitoring research of small scale resistance spot welding based on voltage signal. *ISIJ Int.* 53, 240–244.
- Zhou, K., Cai, L., 2013. Online nugget diameter control system for resistance spot welding. *Int. J. Adv. Manuf. Technol.* 68, 2571–2588.
- Zhou, K., Yao, P., Cai, L., 2015. Constant current vs. constant power control in ac resistance spot welding. *J. Mater. Process. Technol.* 223, 299–304.